Suzaku Observations of Hercules X-1 : Measurements of the Two Cyclotron Harmonics

Teruaki Enoto,[1] Kazuo Makishima,[1,2] Yukikatsu Terada,[2] Tatehiro Mihara,[2]

Kazuhiro Nakazawa,[1] Tsuyoshi Ueda,[1] Tadayasu Dotani,[3] Motohide Kokubun,[3] Fumiaki Nagase,[3]

Sachindra Naik,[3] Motoko Suzuki,[3] Motoki Nakajima,[4] and Hiromitsu Takahashi[5]

[1] *Department of Physics, The University of Tokyo, 7-3-1 Hongo, Bunkyo-ku, Tokkyo 113-0033*

enoto@amalthea.phys.s.u-tokyo.ac.jp

[2] *Cosmic Radiationn Laboratory, The Institute of Physics and Chemical Research (RIKEN),*

2-1 Hirosawa, Wako, Saitama 351-0198

[3] *Institute of Space and Astronautical Science (ISAS), Japan Aerospace Exploration Agency (JAXA),*

Yoshinodai, Sagamihara, Kanagawa 229-8510

[4] *Department of Physics, College of Science and Technology,*

Nihon University, 8-14, Kanda-Surugadai 1-chome, Chiyoda-ku, Tokyo 101-8308

[5] *Department of Physical Science, Hiroshima University,*

1-3-1 Kagamiyama, Higashi-Hiroshima, Hiroshima 739-8526

Abstract

The accretion-powered pulsar Her X-1 was observed with Suzaku twice in its main-on state, on 2005 October 5-6 and 2006 March 29-30, for a net exposure of 30.5 ks and 34.4 ks, respectively. In the 2005 and 2006 observations, the source was detected at an average 10-30 keV intensity of 290 mCrab and 230 mCrab, respectively. The intrinsic pulse period was measured on both occasions at 1.23776 s by HXD-PIN, after barycentric and binary corrections. The pulse phase-averaged spectra in the energy range above 10 keV are well fitted by "Negative and Positive power-law times EXponential (NPEX)" model, multiplied by a fundamental cyclotron resonance scattering feature at ∼36 keV which appears very significantly in the HXD-PIN data. The resonance profiles were reproduced successfully by the Lorentzian type scattering cross section, rather than by a Gaussian type alternative. The pulse phase-averaged HXD-GSO data, covering 50-120 keV, are featureless. However, in a differential spectrum between the pulse-decay phase and off-pulse phase, the second harmonic cyclotron resonance was detected in the GSO data at ∼73 keV, with a depth of $1.6^{+0.9}_{-0.7}$. This makes Her X-1 a 6th pulsar with established second harmonic resonance. Implications of these results are briefly discussed.

1

1. Introduction

Magnetic field strength is one of the important fundamental physical parameters of neutron stars. Their surface magnetic-field strengths can be most accurately determined by measuring quantized electron cyclotron resonances, corresponding to transitions between adjacent Landau levels which are separated by

$$E_\mathrm{a} = 11.6 \; B_{12} \cdot (1+z)^{-1} \quad \mathrm{keV}, \tag{1}$$

where B_{12} is the magnetic field strength in units of 10^{12} Gauss, and z is gravitational redshift. Since this E_a, with $B_{12} \sim 1$ falls in the X-ray energy range, accretion-powered X-ray pulsars provide an ideal laboratory where we can directly measure E_a, and hence B_{12}. Indeed, spectral absorption features at this resonance, called cyclotron resonance scattering features (CRSFs), have so far been detected from more than 15 acceretion-powered X-ray pulsars (e.g., Trumper et al. 1978; Wheaton et al. 1978; Clark et al. 1990; Mihara 1995; Makishimal et al. 1990; Makishimal et al. 1999; Coburn et al. 2002; Salvo et al. 2004). Using equation (1), the surface magnetic field strengths of these pulsars have been found to cluster in a narrow range of (1-5)$\times 10^{12}$ Gauss (Makishimal et al. 1999).

Some of those pulsars with CRSFs exhibit multiple harmonic absorption features. It was reported that 4U 0115+63 has four harmonics (Santangelo et al. 1999; Nakajima et al. 2006), and X0331+63 has up to the third harmonics (Pottschmidt et al. 2005; Tsygankov et al. 2006a; Mowlavial. 2006). In addition, there are objects exhibiting double (fundamental and second harmonic) CRSFs, including Vela X-1 (Kreykenbohm et al. 1998; Makishimal et al. 1999), 4U1907+09 (Cusumano et al. 1998; Makishimal et al. 1999), and A0535+26 (Kendziorra et. al. 1994; Grove et al. 1995).

Since the fundamental and higher harmonic resonances involve somewhat different elementary processes (e.g., Alexander & Mészáros 1991), measurements of centroid energies, depths, and widths of higher harmonics are expected to provide valuable information on the physics of electron vs. photon interaction in the accretion column. Nevertheless, we do not have sufficient understanding as to, e.g., what controls the relative depths between the fundamental and second harmonic CRSFs. Therefore, we still need to enlarge our sample.

The accretion-powered X-ray pulsar Hercules X-1 (Her X-1) is one of the most studied objects of this class, over decades since its discovery in 1972 by Uhuru (Giacconi et al. 1973). At $\sim$35 keV, Her X-1 exhibits a fundamental CRSF, which is the first CRSF discovered among all pulsars (Trumper et al. 1978). Since then, this $\sim$35 keV CRSF has been studied extensively with various X-ray missions, including Ginga (Mihara et al. 1990), BeppoSAX (Dal Fiume et al. 1998), RXTE (Gruber et al. 2001, Coburn et al. 2002) and INTEGRAL (Klochkov et al.

Table 1. Summary of Suzaku observations of Her X-1.

Epoch	Start(UT)	End(UT)	Exposure (ks) [*]	Position
1	2005/10/05 15:12:00	2005/10/06 10:25:00	30.5	XIS nominal
2	2006/03/29 18:12:00	2006/03/30 15:22:00	34.4	HXD nominal

[*] For the HXD, without dead time correction and elimination of buffer flush intervals.

2007). Nevertheless, the presence of the second harmonic CRSF in this object has remained controversial. While the observation with BeppoSAX obtained evidence of the second harmonic at $E_a = 72 \pm 3$ keV in the descending edge of the main pulse peak (Salvo et al. 2004), the INTEGRAL data did not confirm it in 2005 observations (Klochkov et al. 2007).

Since the flux of an X-ray pulsar is known to cut off steeply above an energy of $\sim 1.5 E_a$ (Makishimal et al. 1999), it is generally not easy to detect the second harmonic CRSF at $\sim 2 E_a$. The Hard X-ray Detector (HXD; Takahashi et al 2007; Kokubun et al. 2007) onboard the Suzaku satelite has realized high sensitivity over a broad energy band, employing Si PIN photo-diodes (hereafter HXD-PIN or briefly PIN) and GSO scintillation counts (hereafter HXD-GSO or briefly GSO), which cover the 10-70 keV and 50-600 keV energy ranges, respectively. When the X-ray Imaging Spectrometer (XIS; Koyama et al. 2007) is incorporated, the energy range to be covered expands to three orders of magnitude. Thanks to the high sensitivity in this broad energy band, Suzaku is expected to settle the issue of the second CRSF in Her X-1. In the present paper, we describe detailed pulse phase-averaged and phase-resolved spectroscopy of Her X-1 made with the Suzaku HXD, and report on our confirmation of the second harmonic CRSF.

2. Observations

Her X-1 has three characteristic periods (Nagase 1989); the 1.24 s intrinsic spin period, the 1.7 day binary period of the pulsar together with its optical companion HZ Her, and the 35 day on-off period which is usually attributed to disk precession. In order to observe a high flux state of Her X-1, we need to sample so-called main-on phase in the 35 days periodicity, and avoid the binary eclipses.

We observed Her X-1 twice with Suzaku since its launch. The first observation was made on 2005 October 5 UT 15:12 through October 6 UT 10:25, and the second on 2006 March 29 UT 18:12 through March 30 15:22. These dates were both chosen to observe the main-on phase and to avoid eclipses, in reference to past observations (Zane et al. 2004; Still et al. 2001). In both observations, the HXD was operated in the standard mode, while the XIS employed "1/8 window" option to improve the time resolution (to 1 s) and to avoid event pile up.

Figure 1 shows a long-term light curve of Her X-1 obtained by the RXTE ASM. As indicated there, the two Suzaku observations both sampled the main-on phase as aimed.
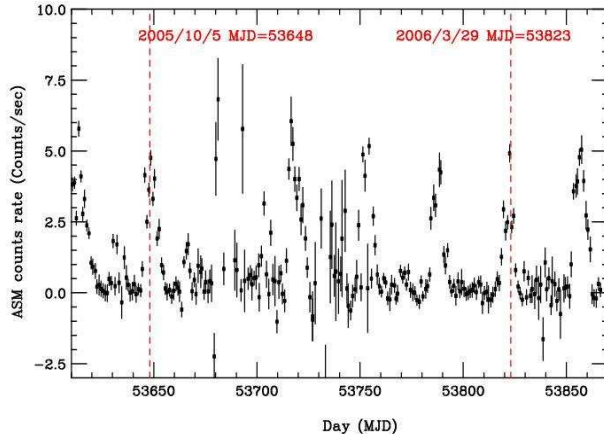
3

Fig. 1. A 2-10 keV light curve of Her X-1 obtained with the RXTE ASM. The two Suzaku observations are indicated with red dashed lines.

3. Data reduction

We analyzed the HXD data prepared via version 1.2 pipeline processing. The data screening criteria we employed are as follows: (a) the time after passage through the South Atlantic Anomaly should be larger than 500 seconds; (b) the target object should be above the earth rim by at least 5°; (c) geomagnetic cutoff rigidity should be greater than 8 GV c^{-1}; and (d) the data should be free from "buffer flash" (Kokubun et al. 2007). The screenings yielded a net HXD exposure of 30.5 ks and 34.4 ks, in the 2005 and 2006 observations, respectively.

Although our main objective is to search the HXD data for the second harmonic CRSF, we briefly utilize the XIS data as well. Therefore, we retrieved the XIS data of the two observations, both processed with version 1.2 pipeline. Figure 2a shows the 0.4-10 keV XIS2 light curves. The XIS background, though included in these light curves, is completely negligible ($\sim 7 \times 10^{-2}$ c s^{-1}). The XIS data were not acquired in the former half of the 2006 observation, due to an operation error. In the 2006 XIS light curve, we find a few occasions of intensity decrease. Since the HXD light curves do not show any corresponding feature, they are likely to be so-called intensity dips, observed occasionally from Her X-1 (Mihara et al. 1991).

Panels (b) and (c) of figure 2 are the background-subtracted and deadtime-corrected light curves from HXD-PIN (10-70 keV) and HXD-GSO (50-100 keV), respectively. Thus, both observations were free from binary eclipses. The source was detected with an average 10-30 keV PIN intensity of 16.9 cnt s^{-1} and 13.1 cnt s^{-1} in the first and second observations, respectively.

We constructed GSO background (bgd_d model) using a method developed by Fukazawa et al. (2007) for the 2005 and 2006 observations. We used this GSO background model to drive the light curves in figure 2 and to perform standard phase average spectrum analysis in §5.1. Although this GSO background model is available only in relatively coarse energy bins, finer binnings can be incorporated in the phase-resolved spectroscopy (§5.2), which does not depend
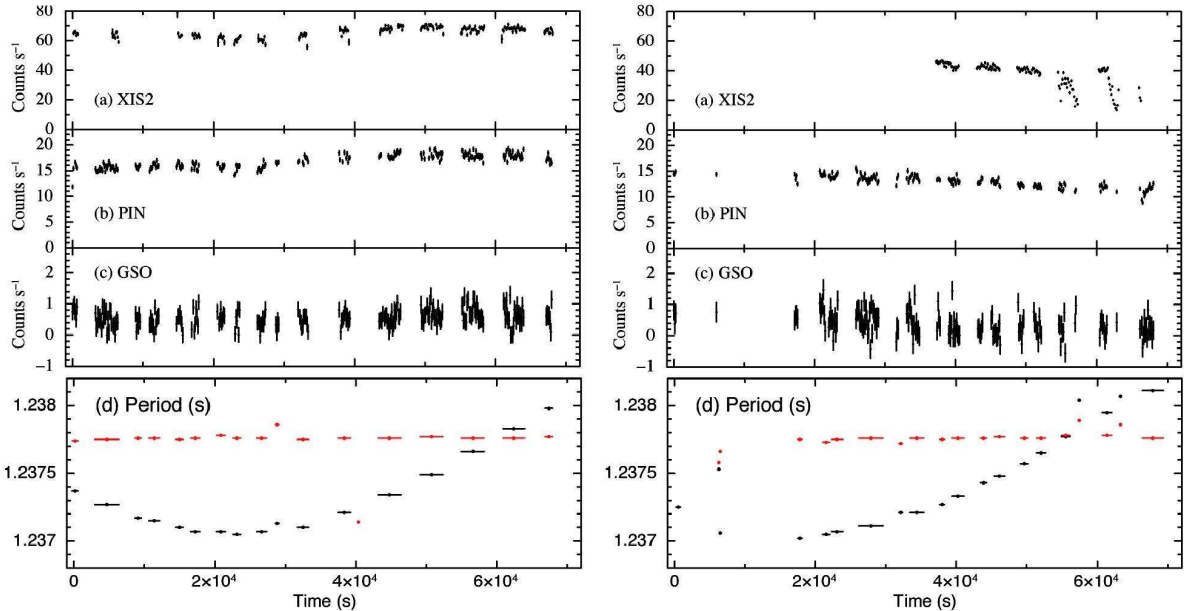
4

Fig. 2. Light curves and period changes of Her X-1 in the 2005 (left) and 2006 (right) observations. (a) Background-subtracted 0.4-10 keV XIS2 light curve. (b) Background-subtracted and dead-time corrected HXD-PIN light curve in the 10-70 keV energy band. (c) The 50-150 keV HXD-GSO light curve, obtained in the same way as the PIN data. (d) The pulsation period determined by the folding analysis of the PIN data at each good time interval, before (black) and after (red) correcting for the binary motion.

on the GSO background model. To analyze the 2005 data, we utilize PIN background model called bgd_a developed by Watanabe et al. (2007), while another model (bgd_d) developed by Fukazawa et al. (2007) for the 2006 PIN data.

4. Timing Analysis

Since the XIS data have a time resolution of 1 s, we conduct the timing analysis only on the HXD data. The arrival time of each HXD event was corrected for the orbital motion effect of the Earth around the Sun, and that of the satellite around the Earth, using a Suzaku specific tool *aebarycen* (Terada et al. 2007) and the object coordinates as $(\alpha,\delta)=(16^{\mathrm{h}}57^{\mathrm{m}}49\overset{\mathrm{s}}{.}83,$ $35°20'32\overset{''}{.}6)$. The bottom panels (black) of figure 2 show the pulse period at each good time interval, determined after these corrections by the standard folding analysis of the 10-70 keV background-inclusive PIN data. The orbital motion of the pulser is clearly seen.

As a next step, we corrected the event arrival times for the orbital delay $\triangle t$ arising in the Her X-1 system, using a formula as

$$\triangle t = \frac{a \sin i}{c} \sin\left[2\pi\left(\frac{t}{P_{\mathrm{orb}}} - \phi_0\right)\right]. \tag{2}$$

Here, a is the semi-mejor axis, i is the inclination, c is the speed of light, t is an event time (suzakutime with its origin on 2000 January 1th UT 00:00), P_{orb} is the orbital period, and ϕ_0

Table 2. Orbital parameters of Her X-1 employed in the present paper (Still et al. 2001).

Parameter	Value
$(a/c) \sin i$ (s)	13.19029
P_{orb} (days)	1.7001673
$\phi_0{}^*$	0.064

* Orbital phase origin, defined using equation (2) at suzaku-time 0.0.

is the phase origin. The values of $(a/c) \sin i$ and P_{orb}, as given in table 2, were employed, while ϕ_0 corresponding to the suzakutime 0.0 was calculated using the phase origin and the values of P_{orb} given by Still et al. (2001). When we scanned ϕ_0 over a range of 0.0-1.0, just for a cross check, periodograms calculated for sufficiently long time intervals ($\sim$30 ks) exhibited the strongest contrast correctly at $\phi_0 \sim 0.064$. As presented in figure 2(a) in red, this orbital-delay correction has brought all the instantaneous period measurements into a constant value, $P_0 = 1.23776$, in both observations, with a typical uncertainty of 1×10^{-5} s. Thus, we quote the intrinsic pulse period of Her X-1 as 1.23776 ± 0.00001 s, both on MJD 53646 and MJD 53823. Any pulse-period difference between the two epochs is comparable to this error.

Figure 3 shows energy-sorted and background-inclusive pulse profiles of Her X-1 in the two observations. These were obtained by folding the data at the period of P_0. In both observations, the pulsation was clearly detected up to 90 keV by the HXD. The measured pulse shapes are typical of the main high state (Deeter 1998). Although they are similar between the two occasions, a trailing shoulder at phase $\sim$0.2 is more prominent in 2005.

5.   Analysis of the HXD Spectra

In this section, the HXD spectra obtained in the two observations are analyzed; the XIS data analysis will be reported elsewhere. We employ a GSO correction factor, which has been introduced by Takahashi et al (2007) to reproduce the Crab spectra by a single power-low model in the 70-300 keV energy range. In addition, we introduce 1% systematic errors in all spectral fitting analyses, to reflect typical uncertainties in the current instrumental calibration. The model normalization is constrained to be the same between HXD-PIN and HXD-GSO, while allowed to take different values between the HXS and HXD. This is because the 1/8 window option of the XIS introduces some uncertainties in the absolute source flux.

5.1.   Phase-averaged spectra

Figure 4 shows the background-subtracted 0.1-100 keV spectra of Her X-1, obtained by the XIS, HXD-PIN and HXD-GSO. Since the 2005 and 2006 data give very similar spectra, we co-added them together in figure 4. The background models (described in §3) used for
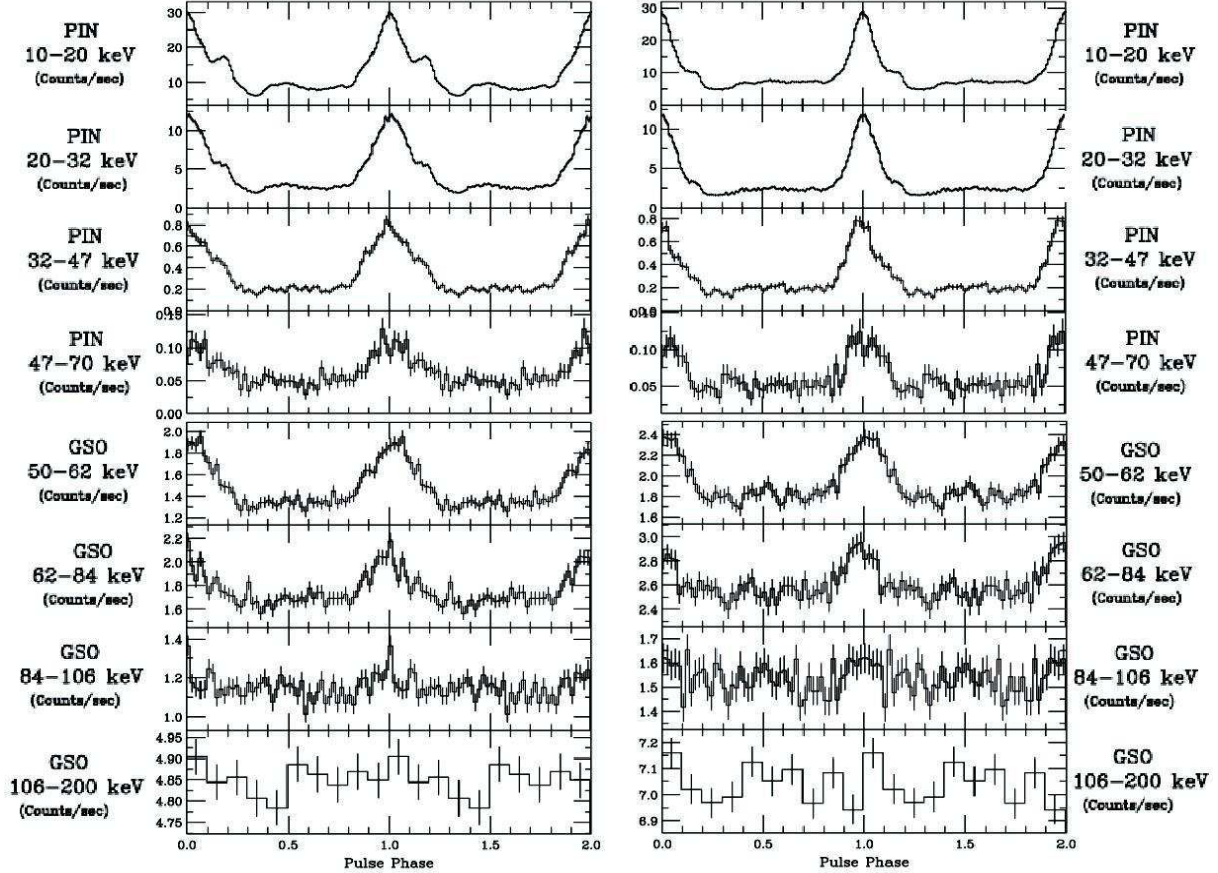
6

Fig. 3. Energy-sorted and background-inclusive pulse shapes of Her X-1 obtained in the 2005 (left) and 2006 (right) observations. The data were folded by the barycenter- and binary-corrected pulse period, $P_0 = 1.23776$ s. The phase zero ($\phi = 0$) is adjusted to the main central peak in the PIN energy band.

the PIN and GSO data are also shown. From the XIS data, we subtracted the night earth backgrounds. After subtracting the background, the summed data yield an average 1–50 keV flux of 6.0×10^{-9} erg cm^{-2} s^{-1}. This value was derived by fitting the XIS, HXD-PIN, and HXD-GSO spectra simultaneously by an empirical model consisting of an NPEX continuum (to be described later), and a low-energy blackbody to reproduce the soft X-ray excess. Assuming an isotropic emission, this implies a 1–50 keV luminosity of 3.1×10^{37} erg s^{-1} at a distance of $D = 6.6 \pm 0.4$ kpc (Reynolds et al. 1997). This luminosity is typical of Her X-1 in the main on state. For reference, the first and second observations yielded the 1–50 keV luminosity of 3.6×10^{37} erg s^{-1} and 2.5×10^{37} erg s^{-1}, respectively.

The HXD spectra in figure 4 are expanded in figure 5a, and are normalized in figure 5b to the Crab spectra acquired with the HXD on 2005 September 15 at the HXD nominal position. Thus, the source intensity averaged over the two observations was ~250 mCrab in the 10-30 keV band. Independent analyses of the 2005 and 2006 data gave the same quantity as ~290 mCrab and ~230 mCrab, respectively. In the Crab ratio, we observe a broad dip at
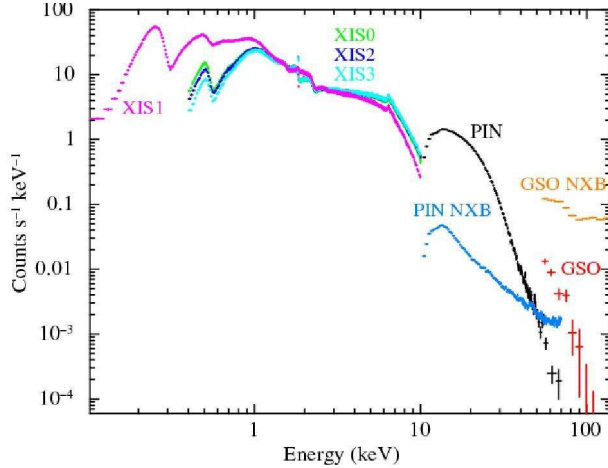
Fig. 4. Background-subtracted and pulse phase-averaged spectra of Her X-1, obtained by the XIS, HXD-PIN, and HXD-GSO. Spectra from the 2005 and 2006 observations are summed up. The non-Xray background models of PIN and GSO are also shown.

∼36 keV, to be identified later with the fundamental CRSF.

To represent the spectral continuum, we employed so-called Negative and Positive power-law times EXponential (NPEX) model, expressed as (Mihara 1995; Makishimal et al. 1999)

$$f(E) = (AE^{-\alpha_1} + BE^{+\alpha_2}) \times \exp(-E/E_{\text{cut}}). \tag{3}$$

Here, E is the energy, $f(E)$ is the photon number spectrum, E_{cut} is a cutoff energy, A and B are normalization factors, while $\alpha_1 > 0$ and $\alpha_2 > 0$ are two photon indices. We adopt $\alpha_2 = 2$ for the positive power-law component, so that the second term represents a Wien hump in a saturated inverse Compton spectrum. First, we fitted the data by this NPEX continuum, but the fit was not acceptable with a reduced chi-square of ∼11. The residuals, shown in figure 5c, exhibits a strong dip around 36 keV. This feature, already noted in figure 5b, is interpreted as the CRSF established through the past studies (§1).

As a next step, we multiplied the NPEX continuum by a factor e^{-S}, where S represents the cyclotron scattering cross section given as

$$S = \frac{DE^2}{(E - E_a)^2 + W^2} \times \left(\frac{W}{E_a}\right)^2, \tag{4}$$

with E_a, D, and W being the energy, depth, and width of the resonance (e.g., Clark et al. 1990, Makishimal et al. 1999). This model has given a fully acceptable fit with a reduced chi-square of 0.51. This value is apparently too small, suggesting a slight over-estimation of the systematic error, but this simply makes our subsequent analysis more conservative. Histograms in figure 5a display this best fit model, and figure 5d shows residuals between the data and the model. The obtained resonance energy $E_a = 35.9^{+0.3}_{-0.3}$ keV, with its depth $D = 1.2^{+0.1}_{-0.1}$ and width $W = 12.2^{+1.5}_{-1.3}$, is generally consistent with the past measurements. The best-fit parameters are summarized in table 3.
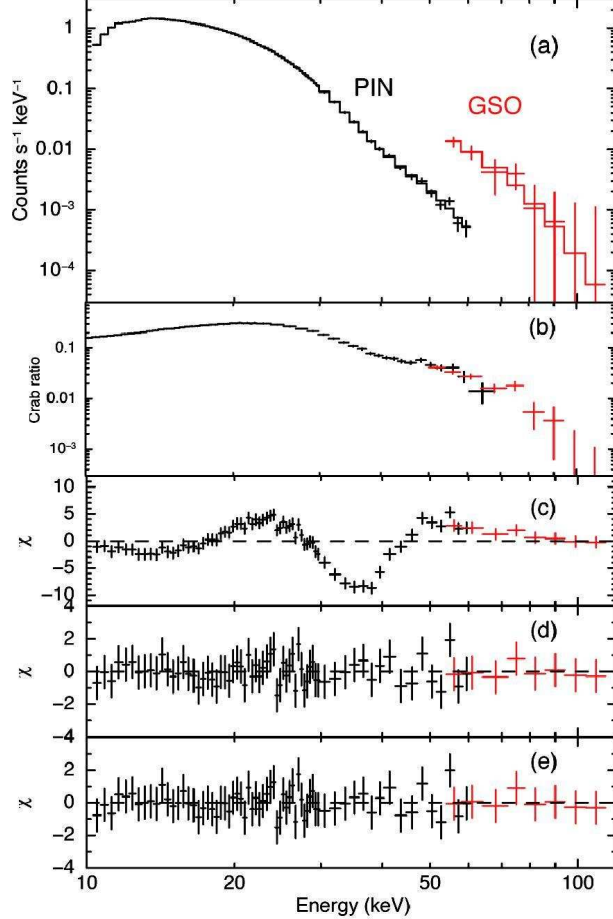
8

Fig. 5. (a) An expanded view of the HXD spectra presented in figure 4. Histograms in the figure represent the best fit model consisting of an NPEX continuum and a fundamental cyclotron resonance. (b) The same spectra, divided by those of the Crab Nebula. (c) Residuals from an NPEX fit. (d) Residuals between the data and the best fit model in panel (a). (e) Those when a second harmonic CRSF is included.

In the same way, we analyzed the 2005 and 2006 spectra separately, and obtained the results as presented in table 3. Thus, the NPEX times single CRSF model is successful on the individual 2005 and 2006 data as well. The value of E_a is consistent, within errors, between the two observations, in which the 10-30 keV counts was different by $\sim30\pm10\%$.

In figure 5b, the Crab ratio suggests a shallow structure at ~70 keV suggestive of the second harmonic CRSF (§1). In order to quantitatively examine this possibility, we introduced a model consisting of an NPEX continuum, multiplied by two CRSF factors both of the form of equation (4). The energy E_{a2} and width W_2 of the second CRSF factor were fixed at $2E_{a1}$ and $2W_{a1}$, respectively (with the suffix 1 specifying the parameters of the first CRSF), while its depth D_2 was left free to vary. However, as presented in figure 5e, this new model did not significantly improve the fit to the 2005+2006 spectrum: the fit chi-square decreased only by 1.2, while the degree of freedom changed from 69 to 68. Therefore, the second harmonic

9

resonance is insignificant, with the 90% upper limit being $D_2 \leq 1.5$. This is not surprising, since figure 5d reveal little evidence for a negative feature at $\sim 2E_a = 72$ keV.

We repeated the same analysis, namely the NPEX times double CRSF fit, on the 2005 and 2006 data separately. The results were essentially the same as before; the chi-square changed from 45.4 ($\nu = 69$) to 44.3 ($\nu = 68$) for the 2005 data, and from 58.4 ($\nu = 69$) to 58.1 ($\nu = 68$) for the 2006 data, implying an insignificant improvement in both cases.

5.2. Phase-resolved spectra

In many pulsars, the continuum spectra, as well as the cyclotron resonance energies and depths, are known to depend significantly on the pulse phase (e.g., Klochkov et al. 2007). Especially in the phase resolved spectra of Her X-1, Salvo et al. (2004) reported a second CRSF at the descending edge of the main pulse peak (§1). We therefore proceed to pulse phase-resolved spectroscopy, using the 2005 and 2006 data summed up to increase statistics. In the present case, the phase-resolved analysis has two additional merits: it allows us to avoid uncertainties in the HXD background models because we can take direct spectral differences between different pulse phases, and to use finer bindings of the GSO data than is specified by the current GSO background model (§2).

Referring to figure 3, we adopted five on-pulse phases as 0.8–0.9, 0.9–1.0, 1.0–1.1, and 1.1–1.2, while the off-pulse phase as 0.2–0.8. The phases 0.8–0.9 and 1.1–1.2 correspond to the soft leading and descending shoulders of the main peak, while those of 0.9–1.0 and 1.0–1.1 correspond to the leading and descending halves of the main hard peak, respectively. The phase resolved spectra, obtained by subtracting that of the off-pulse phase, are shown in figure 6. In these spectra, the PIN and GSO backgrounds are considered to cancel out with a considerably higher accuracy than is available via the model background subtraction ($\sim 5\%$ for PIN and $\sim 2\%$ for GSO), because the pulse period of 1.24 s is sufficiently shorter than the time scales of typical background variations (minutes to hours), and because Her X-1 is not bright to cause significant ($> 1\%$) increases in the HXD dead times. The bottom half of each panel in figure 6 presents the data, divided by the best-fit NPEX times CRSF model determined by the phase-averaged spectra; the model is meant to provide a rough standard for the phase-resolved spectroscopy. Thus, some phase-resolved specra are approximately represented by the phase-averaged NPEX times CRSF model, but in general the spectral shapes depends significantly on the phase.

We fitted the four pulsed-component spectra by an NPEX continuum and a fundamental CRSF model, which has given a satisfactory fit to the phase-averaged data. Table 4 summarizes the best fit parameters for individual on-pulse phases, and figure 7 shows the fit results for the particular phase $\phi = 1.0 - 1.1$. In the case of $\phi = 0.8$–0.9, $\phi = 0.9$–1.0, and $\phi = 1.1$–1.2, we obtained acceptable fits by this model, with $\chi^2_\nu = 1.05$, 0.51 and 0.62, respectively. The fundamental CRSF is highly significant in all these phases, and the derived resonance energy, $E_a = 40.6$ keV ($\phi = 0.8 - 0.9$), $E_a = 39.0$ keV ($\phi = 0.9 - 1.0$), $E_a = 36.5$ keV ($\phi = 1.0 - 1.1$; see figure 7c),
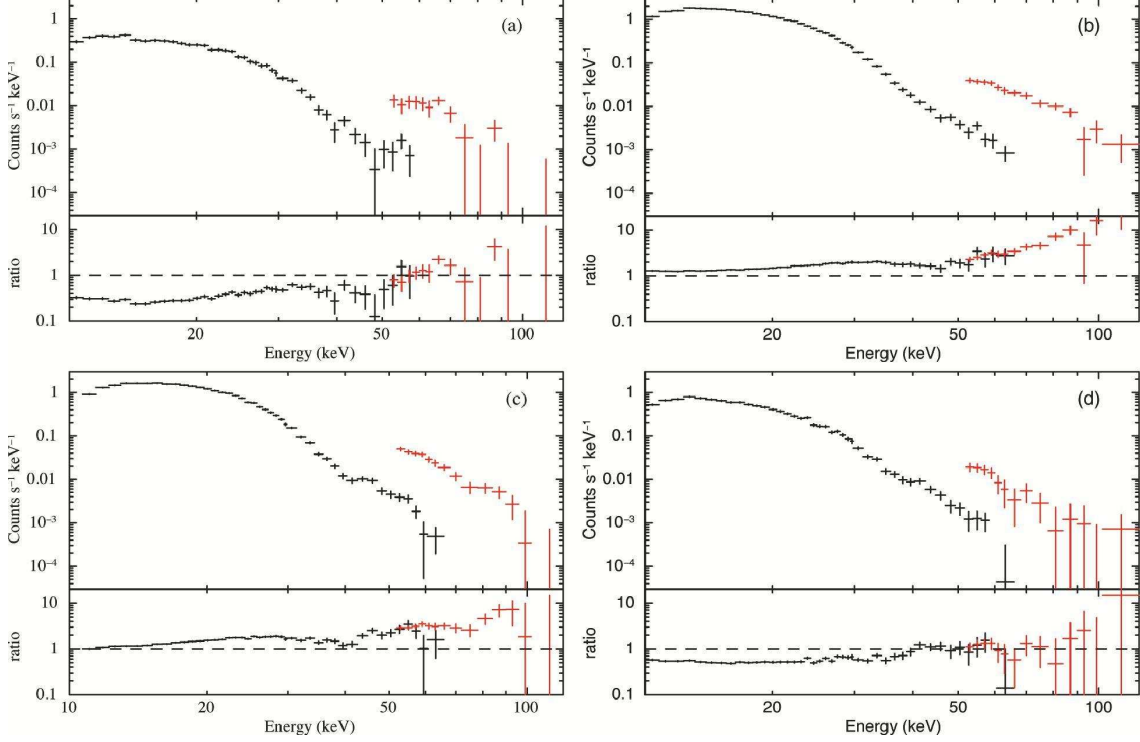
10

Fig. 6. Phase-resolved spectra obtained by subtracting the off-pulse (phase 0.2-0.8) spectrum from on-pulse ones; (a) ϕ =0.8–0.9; (b) ϕ =0.9–1.0; (c) ϕ =1.0–1.1; (d) ϕ =1.1–1.2. The 2005 and 2006 observations are summed up. The bottom half of each panel shows ratios of the data, to the best-fit NPEX times single CRSF model obtained by the phase-averaged spectra.

and 34.8 keV ($\phi = 1.1 - 1.2$), stays within $\sim \pm 10\%$ of that determined with the phase-averaged 2005+2006 spectra. However, as presented in figure 7c, the model failed to reproduce the $\phi = 1.0 - 1.1$ spectra ($\chi^2_\nu = 1.67$), due to significant negative residuals at $\sim$70 keV in the GSO data which is visible even in the ratio between the data and the phase-averaged NPEX times single CRSF model (figure 6c). This can be interpreted as the second harmonic resonance.

We introduced a second CRSF factor, as already performed in §5.1, again with the second resonance energy E_{a2} fixed at $2E_a$. As shown in table 4, the second CRSF factor hardly improved the fits to the $\phi = 0.8 - 0.9$, $\phi = 0.9 - 1.0$, and $\phi = 1.1 - 1.2$ spectra. However, the fit to the $\phi = 1.0 - 1.1$ spectra has been drastically improved from $\chi^2_\nu = 1.67$ to $\chi^2_\nu = 1.07$, and has become acceptable. An F-test indicates that this improvement being cause by chance is $\sim 1.9 \times 10^{-6}$. The second harmonic depth is obtainded as $D_2 = 2.4^{+0.7}_{-1.1}$ (figure 7d). We therefore conclude that the second harmonic CRSF is significantly present in the 2005+2006 spectrum of the pulse phase $\phi = 1.0 - 1.1$.

In order to examine how the present data can constrain the second resonance energy E_{a2}, we repeated the fitting to the $\phi = 1.0 - 1.1$ spectra incorporating the two CRSF factors, but scanning E_{a2} over 55-95 keV. We fixed W_2 at $2W_1$. The behavior of the minimum χ^2, achieved at a given value of E_{a2}, is presented in figure 8. Indeed, the chi-square has reached
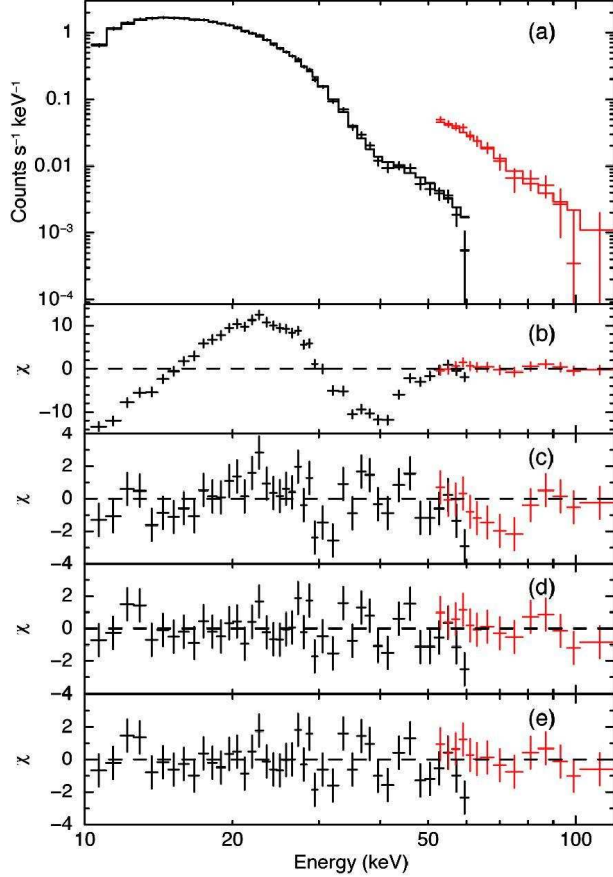
11

Fig. 7. (a) Pulsed-component spectra of Her X-1, obtained by subtracting the data of the off-pulse phase ($\phi = 0.2 - 0.8$) from those of the declining phase ($\phi = 0.0 - 0.1$) of the main pulse peak. Data from the 2005 and 2006 observations are summed up. The histograms in the figure are the best fit model consisting of an NPEX continuum and double cyclotron resonances; corresponding residuals are displayed in panel (e). (b) Residuals when only an NPEX continuum is fitted. (c) Fit residuals from the NPEX×CRSF model, with $E_a = 36.5$ keV. (d) Those with an NPEX and two CRSFs, with E_{a2} fixed at $2E_a$ and W_2 fixed at $2W_1$. (e) The same as panel (d), but E_{a2} is set free.

minimum at ~ 70 keV, where the second CRSF is expected to appear. This ensures that the GSO spectrum at this pulse phase has a significant negative feature at an energy that is close to $2E_a = 73.0 \pm 1.0$ keV at the same pulse phase. This NPEX×2CRSFs model yields the second harmonic resonance energy as $E_{a2} = 70.2^{+6.9}_{-4.6}$, and its depth $D_2 = 1.6^{+0.9}_{-0.7}$ (figure 7e).

So far, the second resonance width W_2 was fixed to twice that of the fundamental. When W_2 is made free to vary, we obtained $W_2 = 29.3^{+\infty}_{-13.9}$ by constraining $E_{a2} = 2E_a$, or $W_2 = 21.9^{+\infty}_{-10.0}$ by allowing E_{a2} to vary freely. Although the upper limit on W_2 thus becomes unbound, the 90% error range of W_2 still includes $2W_1$, confirming the consistency of our assumption.
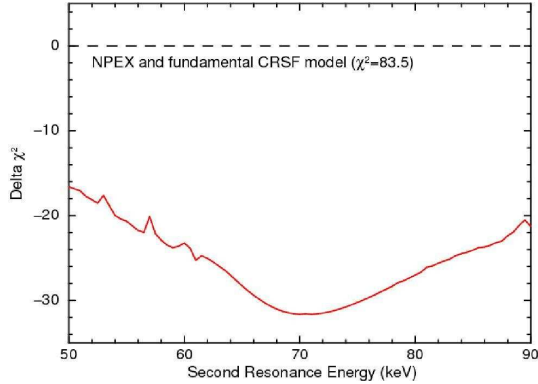
12

Fig. 8. Decrement in the fit chi-square compared to the NPEX×CRSF fit, achieved by adding a second CRSF factor at various energies. The same spectra as presented in figure 7 are used. The width W_2 is fixed at $2W_1$. The chi-square of 83.5 obtained by an NPEX and a fundamental CRSF model is also shown.

6. Discussion

6.1. Pulse periods

We observed Her X-1 twice with Suzaku, in 2005 October and 2006 March, and obtained high-quality data with the HXD and XIS over an extremely broad energy band (0.1–100 keV). On both occasions, Her X-1 showed X-ray intensity and spectra typical in the main-on state of its 35-d cycle.

The intrinsic pulse period was determined with HXD-PIN at 1.23776 ± 0.00001 s on both occasions. This value agrees with the pulse period history of Her X-1 reported by Staubert et al. (2006).

6.2. The fundamental cyclotron resonance

In the pulse phase-averaged HXD-PIN spectra obtained on both occasions, the fundamental CRSF has been detected clearly at ~ 36 keV. Using the NPEX×CRSF spectral model, we have quantified the resonance parameters (table 3, table 4).

Based on multiple observations of Her X-1 with RXTE and other missions, Gruber et al. (2001) and Staubert et al. (2007) argued that its fundamental CRSF energy exhibited long-term variations, possibly related to luminosity changes: after having stayed at ~ 35 keV until 1991, it increased after 1991 to nearly 40 keV, and then it appears to be gradually returning to the previous level. The value of $E_a = 35.9 \pm 0.3$ keV, which we obtained using the pulse phase-averaged 2005+2000 data, is consistent with the pre-1991 value compiled by Staubert et al. (2007), suggesting that the CRSF energy-change episode, whatever the cause be, has come to an end.

Because HXD-PIN has a higher sensitivity at ~ 36 keV than proportional counters, and better energy resolution (~ 3 keV in FWHM) than inorganic scintillator instruments, the present results provide one of the best-quality data on the fundamental CRSF of Her X-1.

13

Importantly, the 10–50 keV PIN spectra bearing the CRSF, including both the phase-averaged and phase-resolved ($\phi = 1.0 - 1.1$) ones, can be reproduced successfully by combining the NPEX continuum of equation (3) with the scattering cross section of equation (4); the CRSF profile has been resolved with a reasonable accuracy. We therefore reconfirm the appropriateness of this modeling, which has been used in many of the past studies of CRSFs including those with Ginga (Clark et al. 1990; Mihara et al. 1990; Mihara 1995; Makishimal et al. 1999), RXTE (Nakajima et al. 2006), INTEGRAL (Tsygankov et al. 2006a), and Suzaku (Terada et al. 2006).

As an exercise, we replaced the cyclotron absorption factor $\exp(-S)$ (S referring to equation 4) with a Gaussian absorption factor used in some other studies (e.g, Staubert et al. 2007; Klochkov et al. 2007); $\exp\left[-a\exp\{(E - E_{\rm c})^2/2\sigma^2\}\right]$, where a, $E_{\rm c}$, and σ are free parameters. When this factor is applied to the NPEX continuum, the fit to the phase-averaged HXD (2005+2006) spectra worsened to $\chi^2_\nu = 0.70$ ($\nu = 69$), from that obtained using equation (4) ($\chi^2_\nu = 0.52$ for $\nu = 69$; table 3). Although this fit is still acceptable (due possibly to an over-estimated systematic error), the Gaussian absorption has failed to reproduce the $\phi = 1.0 - 1.1$ spectra with $\chi^2_\nu = 2.72$ ($\nu = 48$), even when two of them (for the two harmonic CRSFs) were incorporated. Therefore, at least for Her X-1, the Lorentzian-like form of equation (4), which is based on the classical cross section of cyclotron resonance (Clark et al. 1990), is considered more appropriate than the alternative Gaussian cross section.

The above argument may need an important remark: the very deep fundamental CRSF of the transient pulsar X0331+53 (V0332+53), at about 28 keV, cannot be described adequately if using a single form of equation (4) (Makishimal et al. 1990; Nakajima et al. 2006; Tsygankov et al. 2006a). Instead, a nested pair of such absorption factors with different widths (e.g., in terms of Gaussians; Pottschmidt et al. 2005) may be needed.

6.3. Possible origins of the resonance width

What is the origin of the relatively large width of CRSFs, which is generally expressed as

$$W = (0.2 - 0.5)E_{\rm a} \tag{5}$$

(Makishimal et al. 1999; Nakajima et al. 2006)? It has often been argued that W is determined mainly by thermal Doppler effects in the accretion column, including those associated with electron motion along the magnetic field lines (e.g., Dal Fiume et al. 1998; Cusumano et al. 1998; Coburn et al. 2002). However, the failure of the Gaussian optical depth to reproduce the present Suzaku data casts doubt on this interpretation. Furthermore, as pointed out by Makishimal et al. (1999), the values of W of various X-ray pulsars often exceed the expected thermal broadening. According to Nakajima et al. (2006), W_1 of the transient pulsar X0115+63 increased by a factor of ~ 5 as its luminosity changed from 2×10^{36} erg s^{-1} to 5×10^{37} erg s^{-1}, but the temperature of the emission region, $\propto E_{\rm cut}$ of equation (3), increased by only $\sim 20\%$. A similar luminosity dependence of W may be visible even between the present two observations.

These observed changes in W also argue against the thermal broadening scenario.

In explaining W, an obvious alternative is pulse phase-dependent changes in E_{a}. However, in our table 3 and table 4, W_1 is not necessarily smaller in phase-resolved spectra (except in $\phi = 1.1 - 1.2$) than in the phase-averaged ones. Furthermore, the superposition of narrow features with different E_{a} over the pulse phase would not produce wide Lorentzian-like wings. Therefore, this interpretation is not likely, either.

In classical electrodynamics, the width W in equation (4) represents damping effects on the gyrating electrons. In quantum mechanics, the resonance width in this formula generally reflects the finiteness of the life time of excited states, as $W \sim h\Lambda$, through uncertainty principle: here, Λ is transition rate of electrons out of the relevant excited state, and h is the Planck constant. This Λ, in turn, is determined by three competing de-excitation processes; namely, collisional, spontaneous radiative, and stimulated (induced). Among them, the spontaneous transition rate Λ_{rad} (so-called Einstein's A-coefficient) is given as

$$\Lambda_{\mathrm{rad}} \sim 3.8 \times 10^{15} B_{12} \ \mathrm{s}^{-1}$$

(Mészáros 1992), so that the resonance width due to spontaneous emission, namely natural width, becomes

$$W_{\mathrm{nat}} \sim h\Lambda_{\mathrm{rad}} = 15 B_{12} \ \mathrm{eV} = 1.3 \times 10^{-3} E_{\mathrm{a}} \tag{6}$$

where the final form employs equation (1) neglecting the gravitational redshift z. This is still inadequate to explain equation (5). A brief calculation shows that the collisional de-excitation is even less effective.

Let us finally consider the stimulated emission, of which the rate is given as $\Lambda_{\mathrm{st}} = \lambda_{\mathrm{st}} J_{\mathrm{a}}$, where λ_{st} is so-called Einstein's B coefficient, and J_{a} is the radiation energy flux per unit photon frequency at the resonance energy E_{a}; this effect was considered by Alexander & Mészáros (1991). As estimated very crudely in Appendix, Λ_{st} in Her X-1 could be some two orders of magnitude larger than Λ_{rad}. Then, from equation (6), the resonance width due to stimulated emission, $W_{\mathrm{st}} = W_{\mathrm{nat}}(\Lambda_{\mathrm{st}}/\Lambda_{\mathrm{rad}})$, could be a considerable fraction of E_{a}, and might potentially provide an explanation to the observed width. An advantage of this picture is that we can naturally explain the observed positive dependence of W on the X-ray luminosity (Nakajima et al. 2006), because we expect $W_{\mathrm{st}} \propto \Lambda_{\mathrm{st}} \propto J_{\mathrm{a}}$. On the other hand, a caveats is that equation (7) in Appendix predicts the W/E_{a} ratio to decrease steeply toward the higher-field objects, although such a scaling is not necessarily supported by observation. Furthermore, it is not obvious if the absorption feature can be really produced in such a condition as $\Lambda_{\mathrm{st}}/\Lambda_{\mathrm{rad}} \gg 1$, which would usually emhance emission. We leave this intriguing issue to further studies.

6.4. The second harmonic resonance

The pulse phase-averaged HXD spectra did not require the second harmonic resonance, beyond a 90% upper limit of $D_2 \leq 1.5$. However, in the pulse phase-resolved spectra which
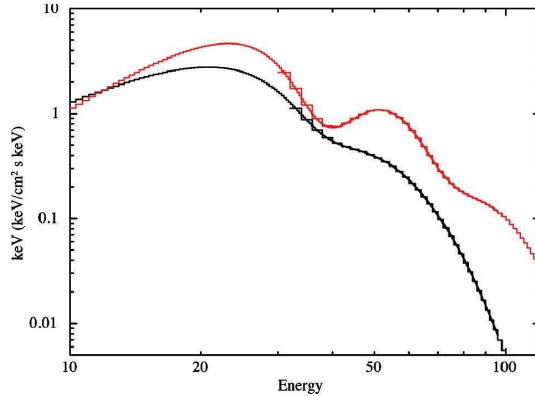
Fig. 9. The best-fit $\nu f \nu$ model spectra. The black line shows the best-fit NPEX continuum multiplied by a fundamental CRSF determined using the 2005+2006 pulse phase-averaged spectrum. The red line shows the best-fit NPEX continuum multiplied by double CRSFs specified by a 2005+2006 pulse phase-resolved spectrum ($\phi = 1.0 - 1.1$).

cover the descending edge of the main pulse ($\phi = 1.0 - 1.1$), we have successfully detected the second CRSF with $D_2 = 2.4^{+0.7}_{-1.1}$ (under the constraints of $E_{a2} = 2E_a$ and $W_2 = 2W_2$). Its energy, when allowed to vary, becomes $E_{a2} = 70.2^{+6.9}_{-4.6}$, yielding $E_{a2}/E_a = 1.9 \pm 0.2$ which satisfies the 1:2 harmonic ratio. Here, the value of E_a can be taken either as the phase-averaged value, or that at this particular pulse phase, because they agree within 2%.

As evidenced by the large chi-square decrements (figure 8), the present detection of the second harmonic feature is statistically highly significant. The feature cannot be artifacts due to systematic errors in the background subtraction (§5.2), since background systematics can be neglected in these "on-pulse minus off-pulse" spectra. Another concern is the uncertainty in the GSO response, toward lower energies (Kokubun et al. 2007). We confirmed that the second harmonic resonance remains significant even when we discard the GSO energy ranges below 60 keV, although errors on the second resonance parameters increase. We therefore conclude that the detected feature is real.

Evidently, HXD-GSO played a major roll in detecting the second CRSF, which lies outside the HXD-PIN energy range. Nevertheless, the PIN data also contributed to its detection, because the inclusion of the second resonance factor has considerably decreased fit residuals in the PIN energy range as well (figure 7c, d, e). In figure 9, we show the inferred best-fit model spectrum for phase-averaged with a fundamental CRSF and for phase-resolved with double CRSFs.

The second CRSF of Her X-1 was first reported by BeppoSAX, from a main-on state observation in October 2000 (Salvo et al. 2004). It appeared in the descending edge of the main pulse peak, with the resonance energy at $E_{a2} \sim 72 \pm 3$ keV and its width $W_2 \sim 11 \pm 1$ keV. Our results agree with those from BeppoSAX, with respect to the resonance energy, as well as the particular pulse phase where it becomes significant. These results hence make Her X-1 a
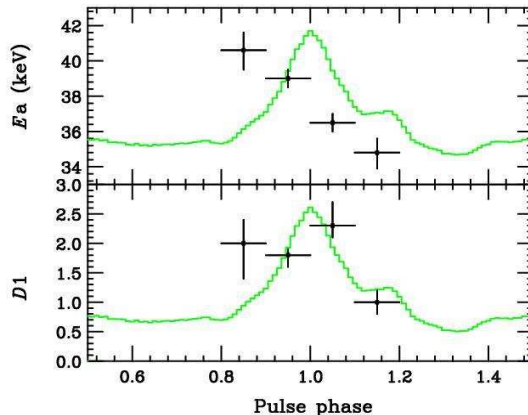
16

Fig. 10. (top) Fundamental CRSF energies presented as a function of the pulse phase, obtained by subtracting the interpulse spectrum from on-pulse ones using the 2005+2006 data. The 10–20 keV pulse profile (also summed over 2005 and 2006) is superposed. (bottom) Fundamental CRSF depths presented in the same manner.

6th pulsar with the second harmonic resonance. The negative detection of this feature with INTEGRAL, in another main-on state observation conducted in July-August 2005 (Klochkov et al. 2007), is probably due to insufficient statistics.

The present results suggest that the second harmonic resonance is a rather common feature of accreting X-ray pulsars, particularly when they are luminous (Nakajima et al. 2006). Even though the cross section of photon vs. electron interaction in a strong magnetic field is much larger at E_a than at $2E_a$, the two-photon effect by Alexander & Mészáros (1991) ensures that the second harmonic feature can appear as strong as the fundamental. That is, the fundamental resonance acts essentially as a photon scattering process, due to very short lifetime of the excited state. In contrast, the second resonance is expected to act as a pure absorption, because an electron excited by two Landau levels will return to the ground state by emitting two photons with energy $\sim E_a$; these photons fill the fundamental feature, and make it shallower.

6.5. Pulse-phase dependence of the resonances

Figure 10 shows the measured E_{a1} and D_1 as a function of the pulse phase; numerical values are given in table 4. The results generally agree with the INTEGRAL measurements (Klochkov et al. 2007). Thus, in the particular pulse phase ($\phi = 1.0 - 1.1$) where the second CRSF was detected, the fundamental resonance is also very deep showing a large value of D_1, together with a relatively low E_{a1} (though not the lowest). Then, how this particular pulse phase relate to the rotational phase of the pulsar?

Although the rotational modulation of E_{a1} does not allow straightforward explanation, we can think of a simple physical effect related to it; the luminosity-dependent change in E_{a1}. In the transient pulsars X0115+63 (Mihara, Makishima & Nagase 2004; Nakajima et al. 2006)

17

and X0331+53 (Tsygankov et al. 2006b; Nakajima 2006), E_{a1} was found to decrease as the luminosity becomes high enough (several times 10^{37} erg s^{-1} or higher). This is presumably because the accretion column then gets taller, so the resonance photosphere, as seen from end-on directions, appears at a higher altitude in the column where the dipole field intensity is lower (Mihara, Makishima & Nagase 2004). If this effect is also taking place in Her X-1, we expect to observe a relatively low value of E_a when looking onto one of the accretion poles. In contrast, when viewing an accretion column relatively side on, we will sample various heights along it, and to measure a higher value of E_a.

Another candidate mechanism to produce the phase-dependent change in E_a is the angle-dependent relativistic effect pointed out by Harding and Daugherty (1991). For $E_a \sim 36$ keV, this effect makes the exact value of E_a to decrease by $\sim 3\%$ at the pole-on phase than at the side-on phase. Although this shift is small, it works in the same sense as the previous one.

In addition to the above two mechanism, yet another effect may also produce the phase dependence of E_a; namely, bulk Doppler effect in the accretion column. Since the accretion flow onto a pulsar has a typical velocity of $v_{fl} \sim c/3$, we expect the post-shock plasma in the radiating accretion column to have a bulk flow of $\sim v_{fl}/4 \sim 0.1c$, at least just beneath the standing shock surface. Then, the longitudinal Doppler shift associated with this bulk flow will make E_a lower by $\sim 10\%$ when we look onto the column, while the effect will vanish at side-on phases. Actually, Terada, Ishida & Makishima (2004) invoked such Doppler shifts in accretion columns of magnetized white dwarfs, and successfully explained the unusually strong atomic emission lines observed from several objects of that kind. In X-ray pulsars, this mechanism is expected to work in the same sense as the above two effects, thus enhancing one another.

From these considerations, we tentatively conclude that the descending half of the main pulse, where E_a is relatively low, corresponds to the phase where we are looking end-on into one of the two accretion poles. This agree with theoretical pulse-profile decomposition by Leahy (2004). According to this work, the descending half corresponds to the pole-on phase of one pole; the pulse profile becomes asymmetric with respect to this phase, due to an addition of fan-beam emission from the other pole which reaches us after affected by gravitational light bending. If this phase assignment is correct, we are to conclude that the second harmonic feature becomes most prominent when we are observing one pole from and end-on aspect. Further comparison with other pulsars, including in particular X0115+63 and X0331+53, would be of great value, though beyond the scope of the present paper.

7.   Conclusion

In this paper, we analyzed the HXD data from two Suzaku observations of Her X-1. The fundamental resonance was clearly detected at ~ 36 keV in the pulse phase-averaged and phase-resolved spectra. The Lorentzian-like form of the resonance was found to be appropriate than the alternative Gaussian cross section. The second resonance feature, though absent ($D_2 \leq 1.5$)

in the phase-averaged spectra, was detected at $\sim$73 keV in the pulse phase-resolved spectra at the descending edge of the main peak.

The authors are grateful to all the members of the Suzaku Science Working group, for their help in spacecraft operation, instrumental calibration, and data processing.

Appendix: Estimation of induced emission

Assuming a local thermal equilibrium, detailed balance relates the Einstein's A and B coefficients as $\lambda_{st} = \Lambda_{rad}(hc)^2/(2E_a^3)$, where the quantities are defined in subsection 6.3. Then, the stimulated transition rate, relative to the spontaneous one, can be written as

$$\Lambda_{st}/\Lambda_{rad} = (hc)^2 J_a/2E_a^3 \quad . \tag{7}$$

Let us next estimate the spectral flux density J_a at 36 keV. The observed flux density per unit energy at E_a, *before* the CRSF factor is applied, is derived from our best fit model to the phase-resolved spectra as 3.6×10^{-10} erg s^{-1} cm^{-2} keV^{-1}. Multiplying this by $4\pi D^2$, where $D = 6.6$ kpc (subsection 5.1) is the distance, we obtain a monochromatic luminosity at $E = E_a$ as $l = 1.8 \times 10^{36}$ erg^{-1} s^{-1} keV^{-1}. Further assuming that the two polar emission regions of Her X-1 can be approximated each by a hemisphere of radius $r \sim 100$ m, we obtain

$$J_a = \frac{l}{4\pi r^2}$$
$$= 3.9 \times 10^{20} \left(\frac{r}{100m}\right)^{-2} \left(\frac{E_a}{36 \text{ keV}}\right)^{-3} \text{keV s}^{-1} \text{ cm}^{-2} \text{ Hz}^{-1}$$

after transforming units from erg keV^{-1} to keV Hz^{-1}. This finally yields

$$\Lambda_{st}/\Lambda_{rad} \sim 62 \left(\frac{r}{100m}\right)^{-2} \left(\frac{E_a}{36 \text{ keV}}\right)^{-3} \quad .$$

References

Alexander, S. G. & Mészáros, P. 1991, ApJ, 372, 562

Clark, G., Woo, J., Nagase, F., Makishima, K., & Sakako, T., 1990, ApJ, 353, 274

Coburn, W., Heindl, W., A., Rothschild, R., E., Gruber, D., E., Kreykenbohm, I., Wilms, J., Kretschmar, P., & Staubert, R., 2002, ApJ, 580, 394

Cusumano, G., di Salvo, T., Burderi, L., Orlandini, M., Piraino, S., Robba, N., Santangelo, A., 1998, A&A, 338, L79

Dal Fiume, D., et al. 1998, A&A, 329, L41

Deeter, J., E., 1998, ApJ, 502, 802

Fukazawa, Y., Watanabe, S., Kokubun, M., et al. 2007, JX-ISAS-SUZAKU-MEMO-2007-02, http://www.astro.isas.jaxa.jp/suzaku/swg/suzakumemo/suzakumemo-2007-02.pdf

Giacconi, R., Gursky, H., Kellogg, E., Levinson, R., Schreier, E., & Tananbaum, H., 1973 ApJ, 184, 227

Grove, J. E., 1995, ApJ, 438,L25

Gruber, D.E., Heindl, W.A., Rothschild, R.E., Coburn, W., Staubert, R., Kreykenbohm, I., & Wilms, J., 2001, ApJ, 562, 499

Harding, A.K., Daugherty, J.K., 1991, ApJ, 374, 687

Kendziorra, E., et al, 1994, A&A, 291, L31

Klochkov, D., et al. 2007, astro-ph 0704.3062v1

Kokubun, M., et al., 2007, PASJ, 59, S53

Koyama, K., et al., 2007, PASJ, 59, S23

Kreykenbohm, I., Kretschmar, P., Wilms, J., Staubert, R., Kendziorra, E., Gruber, D.,E., Heindl, W., A., & Rothschild, R., E., 1998, Astron. Astrophy., 341, 141

Leahy, D., A., 2004, MNRAS, 348, 932

Makishima, K., et al. 1990, ApJ, 365, L59

Makishima, K., et al. 1999, ApJ, 525, 978

Mészáros, P. 1992, High-Energy Radiation from Magnetized Neutron Stars (Chicago University Press)

Mihara, T., Ph.D.theasis in Univ of Tokyo 1995

Mihara, T., Makishima, K., Ohashi, T., Sakao, T., Tashiro, M., 1990, Nature, 346, 250

Mihara, T., Makishima, K., & Nagase, F., ApJ, 610, 390

Mihara, T., Ohashi, T., Makishima, K., Nagase, F., Kitamoto, S., Koyama, K., 1991, PASJ, 43, 501

Mowlavi, N., et al. 2006, A&A 451, 187

Nagase, F., 1989, PASJ, 41, 1

Nakajima, M., 2006, PhD thesis, Nihon University

Nakajima, M., Mihara, T., Makishima, K., & Niko, H., 2006, ApJ, 646, 1125

Pottschmidt, K., et al. 2005, ApJ, 634, L7

Reynolds, A., P., Roche, P., Quaintrell, H., 1997, Astron.Astrophys., 317, L25

Salvo, T., D., Santangelo, A., and Segreto, A., 2004, Nucl.Phys.B (Proc. Suppl.), 132, 446

Santangelo, A., et al. 1999, ApJ, 523, L85

Staubert, R., Schandl, S., Klochkov, D., Wilms, J., Postnov, K., and Shakura, N. I., 2006, AIP Conference Proceedings, Vol. 840, p.65

Staubert, R., Shakura, N. I., Postnov, K., Wilms, J., Rothschild, R., E., Coburn, W., Rodina, L., Klochkov, D., 2007, A&A, 465, L25

Still, M., O'brien, K., Horne, K., et al. 2001, ApJ, 553, 776

Takahashi, H., et al., 2007a, PASJ, submitted.

Takahashi, T., et al., 2007b, PASJ, 59, S35

Terada, Y., Isdhida, M., & Makishima, K. 2004, PASJ 56, 533

Terada, Y., et al. 2006, ApJ, 648L.139T

Terada, Y., et al. 2007, PASJ, submitted.

Trümper, J., Pietsch, W., Reppin, C., Voges, W., Staubert, R., & Kendziorra, E., 1978, ApJ, 336, 960

Tsygankov, S. S., Lutovinov, A. A., Churazov, E. M., & Sunyaev, R. A., 2006a, MNRAS, 371, 19

Tsygankov, S., Lutovinov, A., Churazov, E., & Sunyaev, R., 2006b, 13th Young Scientists' Conference on Astronomy and Space Physics, eds. A. Golovin, G. Ivashchenko, & A. Simon, (Kyiv University

Table 3. Best-fit parameters of the phase averaged spectra of Her X-1.

model*	$A^\dagger$ ($\times 10^{-2}$)	$B^\dagger$ ($\times 10^{-2}$)	α_1	E_{cut} (keV)	E_{a} (keV)	D_1	W_1 (keV)	$E_{\mathrm{a}2}$ (keV)	D_2	$\chi^2_\nu(\nu)$
2005										
NP	< 0.1	0.1	–	5.6	–	–	–	–	–	8.52 (72)
NP×C1	2.8	3.4	$0.4^{+0.7}_{-0.4}$	$7.3^{+0.6}_{-0.6}$	$36.0^{+0.6}_{-0.4}$	$1.5^{+0.2}_{-0.2}$	$15.3^{+2.0}_{-2.1}$	–	–	0.66 (69)
NP×C12	3.0	2.0	$0.1^{+0.6}_{-0.1}$	$8.7^{+2.8}_{-2.0}$	$35.8^{+0.6}_{-0.6}$	$1.8^{+0.2}_{-0.2}$	$16.4^{+1.1}_{-1.6}$	–	$1.0^{+1.0}_{-0.5}$	0.65 (68)
2006										
NP	< 0.1	7.6	—	5.0	–	–	–	–	–	6.9 (72)
NP×C1	0.9	4.6	$1.2^{+2.0}_{-1.2}$	$5.8^{+0.5}_{-0.3}$	$35.5^{+0.5}_{-0.5}$	$0.9^{+0.2}_{-0.1}$	$9.6^{+1.5}_{-1.3}$	–	–	0.85 (69)
NP×C12	0.8	4.6	$1.1^{+1.9}_{-1.1}$	$5.8^{+2.3}_{-0.3}$	$35.3^{+0.3}_{-0.6}$	$0.9^{+0.2}_{-0.1}$	$9.3^{+1.6}_{-1.3}$	–	$0.2^{+0.9}_{-0.2}$	0.85 (68)
sum										
NP	< 0.1	9.7	–	4.9	–	–	–	–	–	10.7 (72)
NP×C1	2.0	4.2	$0.5^{+0.9}_{-0.5}$	$6.4^{+0.5}_{-0.4}$	$35.9^{+0.3}_{-0.3}$	$1.2^{+0.1}_{-0.1}$	$12.2^{+1.5}_{-1.3}$	–	–	0.52 (69)
NP×C12	2.5	2.5	$0.0^{+0.5}_{-0.0}$	$7.4^{+6.3}_{-1.2}$	$35.6^{+0.4}_{-0.5}$	$1.4^{+0.1}_{-0.5}$	$13.6^{+1.4}_{-1.1}$	–	$1.0^{+0.5}_{-0.4}$	0.51 (68)

* NP represents NPEX continum model, C1 represents a foundamental CRSF. C12 represents foundamental and second CRSFs with a second resonance energy fixed at the twice as a foundamental energy, and with the width of a second resonance fixed at the twice as a foundamental one. C1×C2 represents foundamental and second CRSFs with both resonance enrgy free, but with the width of a second resonance fixed at the twice as a foundamental one.
† Referring to equation (3), and defined at 10 keV in unit of counts keV^{-1} cm^{-2} s^{-1}.

Press), p. 115

Watabane, S., Ushio, M., Tanaka, T., Kokubun, M., Fukazawa, Y., et al., JX-ISAS-SUZAKU-MEMO-2007-01, http://www.astro.isas.jaxa.jp/suzaku/swg/suzakumemo/suzakumemo-2007-01.pdf

Wheaton, W. A., et al. 1978, Nature 282, 240

Zane, S., Ramsay, G., Jimenez-Grate, M., A., den Herder, J., W., & Hailey C., J., 2004, MNRAS, 350, 506

Table 4. Best-fit parameters of the phase-resolved 2005+2006 spectra of Her X-1.

model*	$A^\dagger$ $(\times 10^{-2})$	$B^\dagger$ $(\times 10^{-2})$	α_1	E_{cut} (keV)	E_{a} (keV)	D_1	W_1 (keV)	E_{a2} (keV)	D_2	$\chi_\nu^2(\nu)$
ϕ =0.8-0.9										
NP×C1	0.9	6.6	$3.2^{+1.5}_{-1.2}$	$8.0^{+0.8}_{-0.5}$	$40.6^{+1.1}_{-1.0}$	$2.0^{+0.6}_{-0.4}$	$7.5^{+3.4}_{-1.8}$	–	–	1.05 (50)
NP×C12	0.8	2.6	$2.2^{+1.2}_{-0.9}$	$12.6^{+8.1}_{-4.1}$	$40.4^{+1.3}_{-1.3}$	$2.6^{+0.5}_{-0.7}$	$10.9^{+2.7}_{-3.3}$	–	$3.1^{+2.4}_{-2.6}$	0.99 (49)
ϕ =0.9-1.0										
NP×C1	2.1	3.7	$2.2^{+1.4}_{-1.2}$	$7.8^{+0.4}_{-0.3}$	$39.0^{+0.5}_{-0.5}$	$1.8^{+0.2}_{-0.1}$	$11.6^{+2.0}_{-1.3}$	–	–	0.51 (50)
NP×C12	2.4	2.1	$1.1^{+0.9}_{-0.9}$	$10.1^{+4.3}_{-2.3}$	$38.6^{+0.7}_{-0.8}$	$2.2^{+0.3}_{-0.1}$	$13.8^{+1.5}_{-2.0}$	–	$1.4^{+1.5}_{-1.4}$	0.49 (49)
ϕ =1.0-1.1										
NP×C1	< 0.1	4.4	$\cdots$	7.3	37.4	1.9	8.4	–	–	1.67 (50)
NP×C12	0.7	2.3	$0.5^{+13.1}_{-0.5}$	$10.3^{+1.3}_{-1.9}$	$36.5^{+0.5}_{-0.5}$	$2.3^{+0.2}_{-0.4}$	$11.2^{+1.0}_{0.9}$	–	$2.4^{+0.7}_{-1.1}$	1.07 (49)
NP×C1×C2	0.4	3.0	$1.7^{+14.4}_{-1.7}$	$8.9^{+3.3}_{-0.9}$	$36.5^{+0.4}_{-0.2}$	$2.2^{+0.4}_{-0.2}$	$10.2^{+2.0}_{-0.9}$	$70.2^{+6.9}_{-4.6}$	$1.6^{+0.9}_{-0.7}$	1.08 (48)
ϕ =1.1-1.2										
NP×C1	1.9	1.7	$1.2^{+1.4}_{-1.1}$	$6.6^{+0.4}_{-0.3}$	$34.8^{+0.9}_{-0.8}$	$1.0^{+0.2}_{-0.2}$	$4.5^{+2.6}_{1.7}$	–	–	0.62 (50)
NP×C12	1.9	1.7	$1.2^{+1.4}_{-1.1}$	$6.6^{+2.4}_{-0.3}$	$34.8^{+0.8}_{-0.8}$	$1.0^{+0.2}_{-0.2}$	$4.5^{+2.6}_{2.1}$	–	$0.0^{+1.1}_{-0.0}$	0.63 (49)

* Abbreviations and the definition of parameters are the same as in table 3.